Biochemistry

 Volume 39, Number 4 February 1, 2000

Accelerated Publications

Conformational Effects in Biological Catalysis: An Antibody-Catalyzed Oxy-Cope Rearrangement†

Emily C. Mundorff,[‡,§] Michael A. Hanson,[||] Alex Varvak,[||] Helle Ulrich,[‡] Peter G. Schultz,*[,§,||] and Raymond C. Stevens*[,§,||,⊥]

Department of Chemistry, University of California, Berkeley, Berkeley, California 94720, Material Science Division, Lawrence Berkeley National Laboratory, Berkeley, California 94720, and Departments of Chemistry and Molecular Biology, The Scripps Research Institute, 10550 North Torrey Pines Road, La Jolla, California 92037

Received October 20, 1999; Revised Manuscript Received November 24, 2002

ABSTRACT: Antibody AZ-28 was generated against the chairlike transition-state analogue (TSA) **1** and catalyzes the oxy-Cope rearrangement of substrate **2** to product **3**. The germline precursor to AZ-28 catalyzes the reaction with a 35-fold higher rate (k_{cat}/k_{uncat} = 163 000), despite a 40-fold lower binding affinity for TSA·**1** (K_D = 670 nM). To determine the structural basis for the differences in the binding and catalytic properties of the germline and affinity-matured antibodies, the X-ray crystal structures of the unliganded and TSA·**1** complex of antibody AZ-28 have been determined at 2.8 and 2.6 Å resolution, respectively; the structures of the unliganded and TSA·**1** complex of the germline precursor to AZ-28 were both determined at 2.0 Å resolution. In the affinity-matured antibody·hapten complex the TSA is fixed in a catalytically unfavorable conformation by a combination of van der Waals and hydrogen-bonding interactions. The 2- and 5-phenyl substituents of TSA·**1** are almost perpendicular to the cyclohexyl ring, leading to decreased orbital overlap and decreased stabilization of the putative transition state. The active site of the germline antibody appears to have an increased degree of flexibility—CDRH3 moves 4.9 Å outward from the active site upon binding of TSA·**1**. We suggest that this conformational flexibility in the germline antibody, which results in a lower binding affinity for TSA·**1**, allows dynamic changes in the dihedral angle of the 2-phenyl substituent along the reaction coordinate. These conformational changes in turn lead to enhanced orbital overlap and increased catalytic rate. These studies suggest that protein and substrate dynamics play a key role in this antibody-catalyzed reaction.

Studies of catalytic antibodies and their germline precursors make it possible to analyze the evolution of binding energy and catalysis (*1*−*3*). The process of affinity maturation introduces somatic mutations into the antibody that increase binding affinity to hapten. A comparison of the structures of the germline antibody and its affinity-matured counterpart allows one to probe the structural basis for these changes in binding affinity and their effects on catalytic rate. Transition-state theory dictates that rate enhancement should correlate with increased differential binding of the antibody to the transition state relative to substrate (*4*, *5*). The oxy-Cope catalytic antibody AZ-28 and its germline precursor

* Address correspondence to either author.

† Financial support from the Scripps Research Institute, the National Institutes of Health grant AI39089 (to RCS), and the Director, Office of Energy Research, Office of Science, Division of Materials Sciences, of the U.S. Department of Energy under Contract No. DE-AC03-76SF00098.

‡ University of California, Berkeley.
§ Lawrence Berkeley National Laboratory.
|| Department of Chemistry, The Scripps Research Institute.
⊥ Department of Molecular Biology, The Scripps Research Institute.

10.1021/bi9924314 CCC: $19.00
Published on Web 01/04/2000

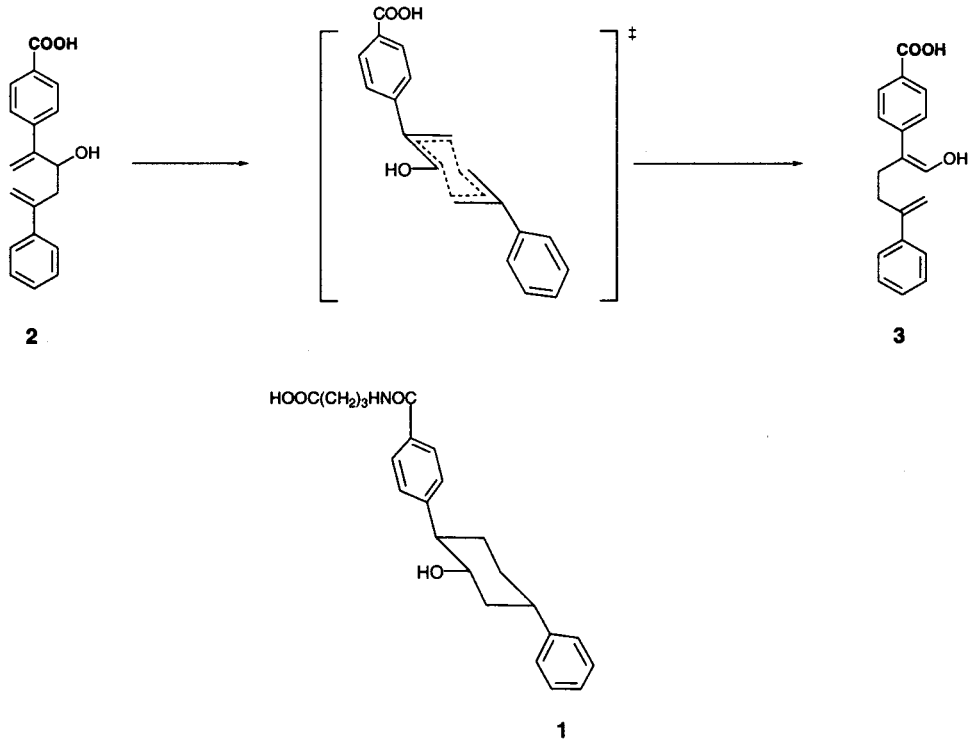

FIGURE 1: Transition-state analogue (TSA·**1**) and the oxy-Cope rearrangement catalyzed by antibody AZ-28.

is one of the few systems where a negative correlation is observed between binding affinity and catalysis. To gain greater insight into additional factors that may affect catalysis in this system, we have carried out a detailed comparison of the three-dimensional structures of the germline and affinity-matured forms of AZ-28.

The oxy-Cope reaction is a unimolecular [3,3] sigmatropic rearrangement (*11*, *12*) that is widely used in organic synthesis but is not catalyzed by any known enzyme. Immunization with TSA·**1** (Figure 1), a chairlike analogue of the putative pericyclic transition state, led to the generation of catalytic antibody AZ-28. This antibody catalyzes the unimolecular oxy-Cope rearrangement of substrate **2** to product **3** with a rate acceleration (k_{cat}/k_{uncat}) of 5300, a K_M of 74 μM, and K_D (**1**) of 17 nM (*13*). The immunological precursor of this antibody was isolated, cloned, and expressed (*2*, *14*, *15*). This germline antibody consists of the T1/B V_L and V_H 19.1.2 germline segments, where V_L and V_H represent the light and heavy chains of the variable domains, respectively (*16*). During affinity maturation (*17*), the germline antibody underwent two amino acid replacements in the light chain (L) [Ser(L34)Asn in complementarity-determining region L1 (CDRL1)[1] and Ala(L51)Thr in CDRL2] and four in the heavy chain (H) [Tyr(H32)Phe in CDRH1, Ser(H56)-Gly and Asn(H58)His in CDRH2, and Thr(H73)Lys in framework region FR3 (Figure 2)]. As expected, the germline antibody has a lower binding affinity for TSA·**1** ($K_D(1)$ = 670 nM) than AZ-28 but, surprisingly, a higher catalytic rate, k_{cat}/k_{uncat} = 163 000 and K_m 73 μM (*2*). To determine which somatic mutations contribute to the higher catalytic rate of the germline antibody relative to AZ-28, the individual somatic mutations were reintroduced into the germline antibody. Analysis showed that whereas five of the six mutations effected the binding affinity, only the Ser(L34)-

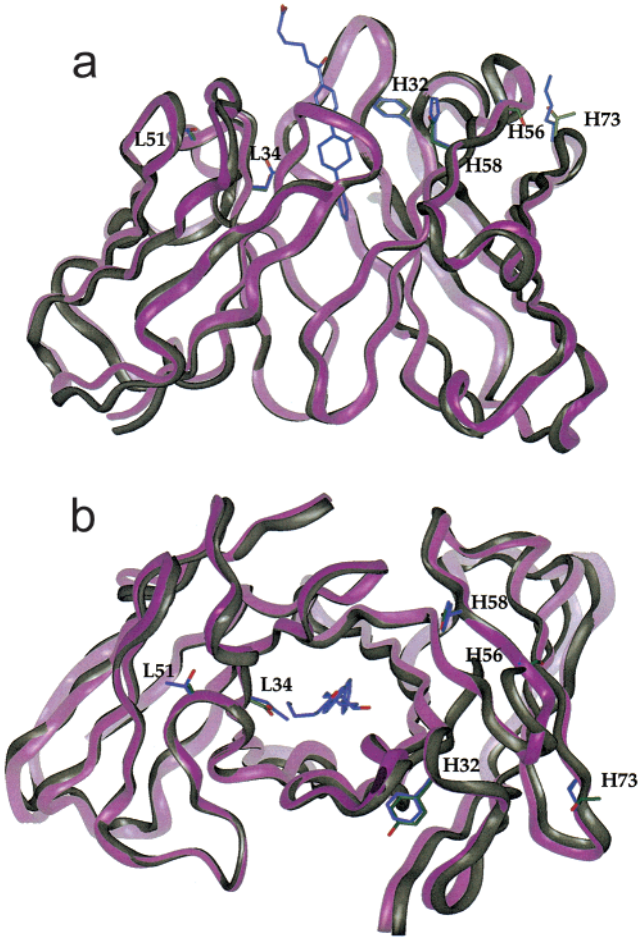

FIGURE 2: (a) Side and (b) top-down view of the superimposed three-dimensional structures of the variable domains of the affinity-matured with hapten (purple) and the unliganded germline (gray).

[1] Abbreviations: TSA, transition-state analogue; CDRH3, complementarity-determining region H3; CDRL1, complementarity-determining region L1.

Table 1: X-ray Data Collection and Refinement Statistics

	mature minus hapten	mature with hapten	germline with hapten	germline minus hapten
resolution (Å)	20.0−2.8	20.0−2.6	20.0−2.0	20.0−2.0
source	SSRL 7−1	SSRL 7−1	ALS 5−2	ALS 5−2
space group	$P2_12_12_1$	$P2_1$	$P2_1$	$P2_1$
unit cell (Å)	77.4 × 80.7 × 134.7	42.8 × 81.5 × 128.3 $\beta = 93.4$	52.7 × 64.4 × 73.9 $\beta = 99.1$	53.2 × 64.1 × 76.0 $\beta = 99.5$
measured reflections	103 369	72 441	66 483	74 105
unique reflections	196 06	25 889	28 062	30 863
completeness (%)	91.2 (70.5)[a]	95.2 (90.5)	85.2 (83)	90.3 (90.5)
R_{merge} (%)	8.0 (28.0)	5.5 (10.6)	7.6 (17.6)	4.0 (14.0)
average I/σ	22 (4)	25 (10)	12 (7)	27 (7)
R_{factor} (%)	23.1	22.8	22.4	21.5
R_{free} (%)	28.5	26.2	26.5	26.4
total no. of atoms	6701	6772	3486	3507
no. of water molecules	59	78	146	193
rms bond lengths (Å)	0.010	0.007	0.023	0.019
rms bond angles (deg)	1.60	1.36	2.27	2.07

[a] Numbers in parentheses are for highest resolution bin.

Asn produced a significant change in the catalytic rate (*2*).

EXPERIMENTAL PROCEDURES

The data collection and refinement statistics are shown in Table 1. The crystals of the germline and affinity-matured Fab fragment of AZ-28 in the presence and absence of TSA·**1** were obtained by the hanging drop method. Crystallization solutions were 10 mg/mL protein in aqueous 100 mM NaCl, 10 mM Tris, pH 8.0, and 1 mM methionine. The mother liquors were aqueous 25% PEG 1000, 100 mM sodium acetate, pH 4.6, 300 mM cadmium chloride, and 100 mM ammonium sulfate for the AZ-28 crystals and were 24 mM cadmium chloride, 75 mM Hepes, pH 7.0, 160 mM ammonium sulfate, 16% 1,4-butanediol, and 8% PEG 8000 for the unliganded germline crystals. The germline antibody·hapten complex was crystallized in the presence of 2 mM TSA·**1** in 80 mM cadmium chloride, 75 mM Hepes, pH 7.0, 250 mM ammonium sulfate, 20% 1,4-butanediol, and 9% PEG 4000. For data collection, the AZ-28 crystals were cryocooled in liquid nitrogen after a brief washing in 15% glycerol and 85% mother liquor. The mother liquor was sufficient cryoprotectant for the germline crystals. All data were integrated and merged using Denzo and Scalepack (*6*). The structures were solved by molecular replacement using the AMoRe package (*7*) with the coordinates of AZ-28 antibody·hapten complex structure for the search model. The model was completed with several cycles of positional, simulated annealing and torsional refinement in CNS (*8*), with NCS restraints in the unliganded affinity-matured structure. Free *R* values were monitored throughout the model building. Maps were produced using CCP4 (*9*) and CNS and interpreted in O (*10*). The affinity-matured antibody·TSA·**1** structure was refined using CNS. There are two molecules per asymmetric unit in the unliganded AZ-28 crystal form. The final structure of unliganded AZ-28 contains 6701 amino acids, 59 water molecules, and 1 Cd^{2+} ion. The germline structures crystallized with one molecule in the asymmetric unit. The final structure of the germline·hapten complex contains 3486 amino acids, 146 water molecules, and 4 Cd^{2+} ions. The unliganded germline structure contains 3507 amino acids, 193 water molecules, and 3 Cd^{2+} ions. All coordinates and structure factors have been deposited to the PDB. The PDBID codes are 1AXS for the AZ-28·hapten complex, 1D5I for the unliganded germline structure, 1D5B for the unliganded AZ-28, and 1D5C for the germline·hapten complex.

RESULTS

Structural Analysis of the AZ-28·Hapten and Germline·Hapten Complexes. The structure of the affinity-matured antibody AZ-28 with TSA·**1** has been previously determined at 2.6 Å resolution (*2*). TSA·**1** is bound in a chairlike geometry with the aryl and hydroxyl substituents of the cyclohexyl ring in equatorial positions. The phenyl substituents of TSA·**1** are rotated with respect to each other by a dihedral angle of 19° and make extensive contacts with active-site residues (Figure 3a). The 5-phenyl group of TSA·**1** is buried at the bottom of the cavity in a hydrophobic pocket. The 2-phenyl substituent is located near the opening of the active site, and its orientation is fixed by a π-stacking interaction with the imidazole ring of His-H96 and van der Waals interactions with the side chain of Tyr-L91. The cyclohexyl ring of TSA·**1**, which mimics the cyclic $4\pi + 2\sigma$ transition state, is rotated out of the planes of the 5- and 2-phenyl rings by 81° and 83°, respectively. Its position is fixed by hydrogen bonding between the hydroxyl substituent of TSA·**1** and both the imidazole ring and the backbone amide NH group of His-H96, in addition to a hydrogen bond through a bridging water molecule to the carboxylate moiety of Glu-H50. The cyclohexyl ring of TSA·**1** is in van der Waals contact with the hydrophobic side chains of Tyr-L91, Tyr-L96, and Tyr-H100a and the hydrophilic side chains of Asn-L34 and Asp-H101. The carboxamide group of Asn-L34 is 3.8 Å from the cyclohexyl ring and makes a 2.6 Å hydrogen bond to the hydroxyl group of Tyr-H100a and a 2.5 Å hydrogen bond to the carboxylate moiety of Asp-H101.

The structure shows that the antibody binds the TSA in a chairlike conformation. This is consistent with the preferred transition state of the oxy-Cope rearrangement (*12*) and places the hexadiene in favorable orbital alignment. This has been confirmed by nuclear magnetic resonance studies of the antibody−substrate Michaelis complex (*18*). Electronic effects, such as hydrogen bonds between the hydroxyl moiety of the substrate and His-H96 and the bridging water to Glu-H50 may lead to increased electron density on the oxygen, thereby accelerating the reaction through an oxyanion

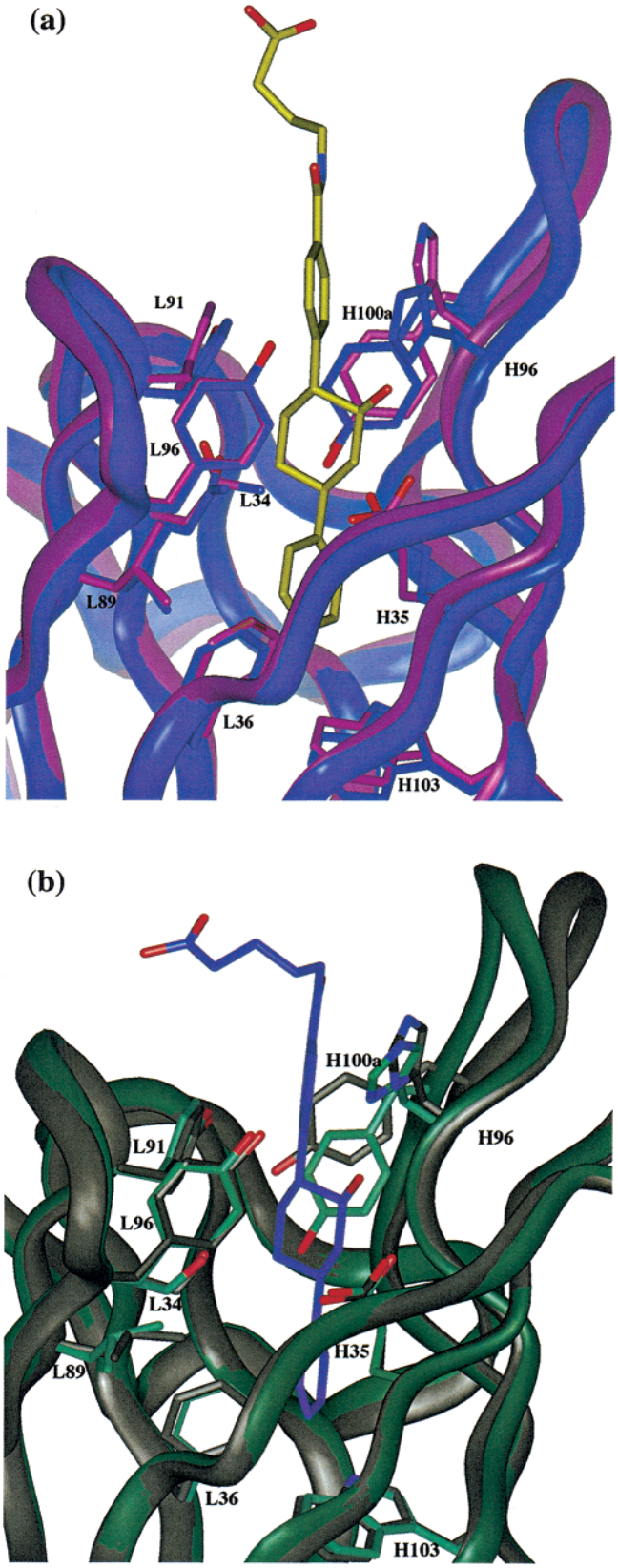

FIGURE 3: (a) Overlay of the active site for the affinity-matured antibody structures with and without hapten present. The affinity-matured antibody with hapten is shown in purple with the hapten in yellow. The unliganded antibody is shown in blue. (b) Overlay of the active site for the germline antibody structures with and without hapten in gray and green, respectively. The hapten is blue.

substituent effect (*19*). It has been shown that the aryl substituents at the 2 and 5 positions of the 1,5-hexadiene lower the activation energy by 5−10 kcal/mol due to stabilization of a biradicaloid-like transition state (*12*). However, the crystal structure shows that the aryl substituents of TSA·**1** are rotated out of planarity with the cyclohexyl ring, leading to decreased π-orbital overlap. This out-of-plane conformation is fixed through the hydrogen-bonding and van der Waals interactions to the cyclohexyl ring along with π-stacking interactions between the 2-aryl substituent and His-H96, Tyr-L91, and Tyr-H100a. On the basis of this analysis, it appears that the substrate is fixed in a catalytically unfavorable conformation. This stems from the fact that the dihedral angles of the 2- and 5-aryl substituents were not restricted in TSA·**1** to be coplanar with the cyclohexyl ring. The antibody likely binds TSA·**1** in its low-energy conformation in solution, with the phenyl rings rotated out of planarity.

To assess the structural basis for the decreased affinity but increased catalytic efficiency of the germline antibody, we determined the three-dimensional crystal structures of the germline antibody with and without TSA·**1**. The hapten in the germline complex is bound in a conformation similar to that seen in the affinity-matured antibody TSA·**1** complex. The cyclohexyl ring of the hapten in the germline structure is stabilized by a 3.0 Å hydrogen bond between the hydroxyl moiety and His-H96, in contrast to three hydrogen bonds to the hydroxyl moiety in AZ-28. The van der Waals contacts between the hapten and the antibody are similar to those seen in AZ-28. The cyclohexyl ring makes van der Waals interactions with the hydrophobic residues Tyr-L91, Tyr-L96, and Tyr-H100a as well as the hydrophilic residues Glu-H35 and Asp-H101. The 2-phenyl substituent is stabilized by van der Waals interactions between Tyr-L91 and Tyr-H100a and by π-stacking interactions with His-H96. There are two water-bridged hydrogen bonds from the hydroxyl group of Ser-L34 to the side chains of Tyr-H100a and Tyr-H101. In the affinity-matured antibody, Asn-L34 forms the same hydrogen bonds but without the bridging water molecule. The 5- and 2-phenyl moieties of the hapten are rotated with respect to the cyclohexyl ring by dihedral angles of 63.2° and 57.9°, respectively, less than that observed in the AZ-28·hapten complex.

The somatic mutations appear to increase the binding affinity of the affinity-matured antibody predominantly through secondary sphere hydrogen-bonding interactions (Figure 2). No individual mutation significantly affects the binding affinity, rather the overall effect appears to result from additive interactions. The mechanism by which the individual mutations increase the affinity to the hapten is not evident from these structures. The sole somatic mutation that resides in the active site is Ser(L34)Asn. This is also the only mutation that significantly affects k_{cat}, although it does not alter K_M. Asn-L34 makes a 2.6 Å hydrogen bond to Tyr-H100a in the AZ-28 antibody·hapten complex, which increases to a 3.5 Å water-bridged hydrogen bond between Ser-L34 and Tyr-H100a in the germline antibody·hapten complex. This is one of the few interactions between the light and heavy chains in the active site and a common point of somatic mutations (*17*).

Structural Effects of Hapten Binding in the Germline and Affinity-Matured Antibodies. A comparison of the unliganded and liganded forms of the germline and affinity-matured antibodies provides insights into conformational changes that

occur upon hapten binding. In the unliganded germline antibody structure, CDRH3 (residues His-H96 to Asp-H101) has a different conformation than that observed in the germline antibody·hapten complex (Figure 3b). Residue Phe-H99 (C_α) at the top of the loop is shifted 4.9 Å away from the hapten in the germline antibody·hapten complex relative to the unliganded structure. The hydrogen bond between Ser-L34 and Tyr-H100a is 3.0 Å, shorter than in the structure of the germline·hapten complex. The imidazole ring of His-H96 is rotated 10° toward the plane of the 2-phenyl ring of the hapten in the germline·hapten complex relative to the unliganded structure. There is no hydrogen bond between Ser-L34 and Tyr-H101 in the unliganded germline antibody, whereas in the germline·hapten complex there is a water-bridged hydrogen between these residues. In both of the germline antibody structures there is minimal density for residues H98−H100, indicating that this region of the loop is disordered.

In contrast to the differences observed between the unliganded germline and germline·hapten structures, few changes occur upon binding of the hapten to AZ-28 (Figure 3). The CDRH3 loop region of the unliganded affinity matured antibody is similar to that of the AZ-28·hapten complex, with the exception of residues H96 and H97. The side chain of His-H96 in the AZ-28·TSA·**1** structure is closer to the hapten with $\chi 1$ rotated 45° toward the plane of the 2-phenyl ring relative to the unliganded structure. In the unliganded structure there is a 3.2 Å hydrogen bond between Asn-L34 and Tyr-H100a, 0.8 Å shorter than that between Asn-L34 and H100a in the liganded structure. Although the side chain density is weak in CDRH3, the backbone density for this loop in both affinity-matured structures is well defined.

Structural Basis for Catalytic Properties of the Germline and Affinity-Matured Antibodies. The structural differences between these four antibody structures are small. The most significant differences are located in CDRH3, at the site of the catalytically important somatic mutation Ser(L34)Asn, and in the conformation of the hapten itself. The CDRH3 loop plays an essential role in binding hapten as it does for the majority of antibodies (*20*). Residues H97−H100a are in a similar conformation in both the unliganded and the liganded affinity-matured structures. In contrast, this region is shifted 4.9 Å out of the active site in the germline antibody·TSA·**1** complex versus the unliganded germline structure (Figure 4). The density for this loop is improved in both of the affinity-matured structures when compared to the germline structures, despite a decrease in resolution, consistent with a higher degree of flexibility in the CDRH3 in the germline structure. In the structures of the unliganded germline and affinity-matured antibodies, the distances between residue L34 and Tyr-H100a are 3.0 and 3.2 Å, respectively (Figure 4). The distance between residue L34 and Tyr-H100a is 2.6 Å in the affinity-matured antibody and increases to 3.5 Å in the germline·hapten complex. The outward displacement of CDRH3 in the germline-TSA·**1** complex relative to the affinity-matured antibody TSA·**1** complex also likely contributes to the decreased dihedral angles of the 2- and 5-phenyl substituents.

The short hydrogen bond in the affinity-matured antibody·TSA·**1** complex appears to stabilize the conformation of CDRH3, which fixes the substrate in a catalytically unfavorable conformation. This in turn would lead to a greater energetic barrier for the chemical step of the AZ-28-catalyzed reaction. Indeed the entropy of activation ($\Delta S^{\ddagger}$) of the AZ-28-catalyzed reaction is -24 ± 8 cal/mol K (the $\Delta S^{\ddagger}$ for the uncatalyzed reaction is -4 ± 9 cal/mol K) (*18*), consistent with considerable conformational reorganization in the active site involving substrate, protein, and/or solvent. In contrast, increased flexibility of CDRH3 in the germline structure leads to a more open active-site structure in the germline antibody·TSA·**1** complex. This lowers the rotational barrier around the 2-phenyl-C2 bond and allows increased π-orbital overlap in the transition state. The net result is an increase in catalytic rate for the germline antibody relative to the affinity-matured antibody. At the same time, this conformational flexibility is most likely responsible for the decrease in binding affinity for the hapten.

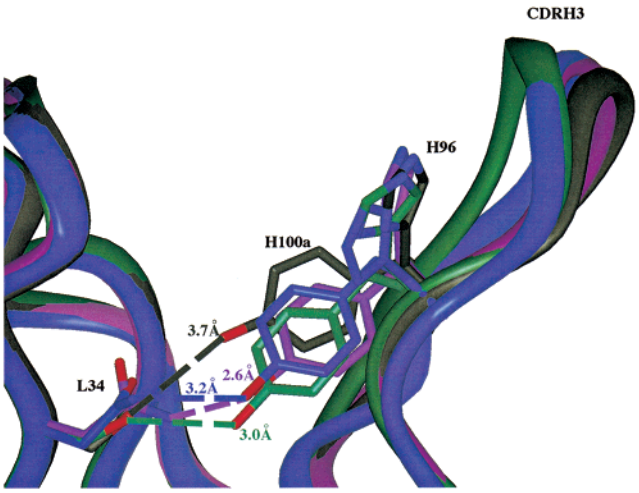

FIGURE 4: Close-up view of the residues Ser(L34)Asn, Tyr-H100a, and His-H96 in a superposition of the four antibody structures. The structures are shown in purple, blue, dark gray, and green for the liganded and unliganded affinity-matured antibody and the liganded and unliganded germline antibody, respectively.

DISCUSSION

As is evident from these studies, the hapten is not a true mimic of the oxy-Cope transition state. The lowest energy conformation for TSA·**1** in the affinity-matured antibody active site is with both aryl substituents perpendicular to the cyclohexyl ring. However, a coplanar arrangement of the aryl substituents with the $4\pi + 2\sigma$ orbitals leads to enhanced orbital overlap and a decrease in free energy of reaction. The increased binding affinity of the affinity-matured antibody stabilizes the substrate in a catalytically unfavorable conformation. In contrast, the more open active-site structure of the germline antibody lowers binding affinity and likely facilitates dynamic changes in substrate conformation during the reaction. Specifically the 2-phenyl-C2 dihedral angle leads to enhanced orbital overlap and increased catalytic efficiency. These studies suggest that conformational dynamics involving both the protein and the substrate can play a critical role in biological catalysis. Indeed, a number of enzymes undergo conformational change upon binding of substrate (*21*) that lead to enhanced catalytic rate, including hexokinase (*22*, *23*) and triosephosphate isomerase (*24*). Recent single molecule kinetic studies of enzyme-catalyzed reactions also suggest that different conformational states of

proteins are characterized by different catalytic rates (*25*). The static snapshots of the oxy-Cope catalytic antibodies described here suggest that conformational isomerization can play an important role in accommodating changes in protein−substrate complementarity that must occur along a complex reaction coordinates involving substrate binding, multiple stereoelectronic effects in the transition state, and product release (*26*). Further studies with NMR are underway to provide additional support for this dynamic model of catalysis suggested by the X-ray crystallographic analysis of antibody AZ-28 and its germline precursor. In addition, it will be of interest to compare the catalytic efficiency of an antibody generated against a rigid coplanar TSA relative to the flexible germline precursor of AZ-28.

REFERENCES

1. Wedemayer, G. J., Patten, P. A., Wang, L. H., Schultz, P. G., and Stevens, R. C. (1997) *Science 276*, 1665−1669.
2. Ulrich, H. D., Mundorff, E. C., Santarsiero, B. D., Driggers, E. M., Stevens, R. C., and Schultz, P. G. (1997) *Nature 389*, 271−275.
3. Romesberg, F. E., Spiller, B., Schultz, P. G., and Stevens, R. C. (1998) *Science 279*, 1929−1933.
4. Pauling, L. (1946) *Chem. Eng. News 24*, 1375.
5. Haldane, J. B. S. *Enzymes* (1930) Longmans, Green & Co, London.
6. Otwinowski, Z., and Minor, W. (1996) *Methods Enzymol. 276*, 307−325.
7. Navaza, J. (1997) *Acta Crystallogr. A 50*, 157−163.
8. Brunger, A. T. (1992) *Nature 355*, 472−474.
9. Collaborative Computational Project Number 4. (1994) *Acta Crystallogr. D 50*, 760−763.
10. Jones, T. A., Zou, J.-Y., Cowan, S. W., and Kjeldgaard, M. (1991) *Acta Cyrstallogr. A 47*, 110−119.
11. Doering, W. v. E., and Roth, W. R. (1962) *Tetrahedron 18*, 67−74.
12. Dewar, M. J. S., and Wade, L. E. (1977) *J. Am. Chem. Soc. 99*, 4417−4424.
13. Braisted, A. C., and Schultz, P. G. (1994) *J. Am. Chem. Soc. 116*, 2211−2212.
14. Ulrich, H. D., Patten, P. A., Yang, P. L., Romesberg, F. E., and Schultz, P. G. (1995) *Proc. Natl. Acad. Sci. U.S.A. 92*, 11907−11911.
15. Ulrich, H. D., Driggers, E. M., and Schultz, P. G. (1996) *Acta Chem. Scand. 50*, 328−332.
16. Kabat, E. A., Wu, T. T., Perry, H. M., Gottesman, K. S., and Foeller, C. *Sequences of Proteins of Immunological Interes*t (1991) U.S. Department of Health and Human Services, National Insitutions of Health, Bethesda, MD .
17. Pech, M., Hochtl, J., Schell, H., and Zachau, H. G. (1981) *Nature 291*, 668−670.
18. Driggers, E. M., et al. (1998) *J. Am. Chem. Soc. 120*, 1945−1958.
19. Steigwald, M. J., Goddard, W. A., and Evens, D. A. (1979) *J. Am. Chem. Soc. 101*, 1994−1997.
20. Kuby, J. *Immunology*, 3rd ed. (1997) W. H. Freeman and Co, New York.
21. Koshland, D. E. (1987) *Cold Spring Harbor Symp Quantum Biol. 52*, 1−7.
22. Anderson, W. F., and Steitz, T. A. (1975) *J. Mol. Biol. 92*, 279.
23. DelaFuente, G., and Sols, A. (1970) *Eur. J. Biochem. 16*, 234.
24. Knowles, J. (1991) *Nature 350*, 121−124.
25. Xie, S., and Lu, H. P. (1999) *J. Biol. Chem. 274*, 15967−15970.
26. Kraut, J. (1988) *Science 242*, 533−540.

BI9924314